analytical chemistry

pubs.acs.org/ac Article

# Solvatochromic Buffering Fluorescent Probe Resolves the Lipid Transport and Morphological Changes during Lipid Droplet Fusion by Super-Resolution Imaging

Ning Xu, Qinglong Qiao,* Xiangning Fang, Guangying Wang, Kai An, Wenchao Jiang, Jin Li, and Zhaochao Xu*

Cite This: *Anal. Chem.* 2024, 96, 4709−4715 Read Online

ACCESS | Metrics & More | Article Recommendations | Supporting Information

**ABSTRACT:** The varied functions of lipid droplets, which encompass the regulation of lipid and energy homeostasis, as well as their association with the occurrence of various metabolic diseases, are intricately linked to their dynamic properties. Super-resolution imaging techniques have emerged to decipher physiological processes and molecular mechanisms on the nanoscale. However, achieving long-term dynamic super-resolution imaging faces challenges due to the need for fluorescent probes with high photostability. This paper introduces **LD-CF**, a "buffering probe" for imaging lipid droplet dynamics using structured illumination microscopy (SIM). The polarity-sensitive **LD-CF** eliminates background fluorescence with a "cyan filter" strategy, enabling wash-free imaging of lipid droplets. In the fluorescent "off" state outside droplets, the probes act as a "buffering pool", replacing photobleached probes inside droplets and enabling photostable long-term SIM imaging. With this probe, three modes of lipid droplet fusion were observed, including the discovery of fusion from large to small lipid droplets. Fluorescence intensity tracking also revealed the direction of lipid transport during the lipid droplet fusion.

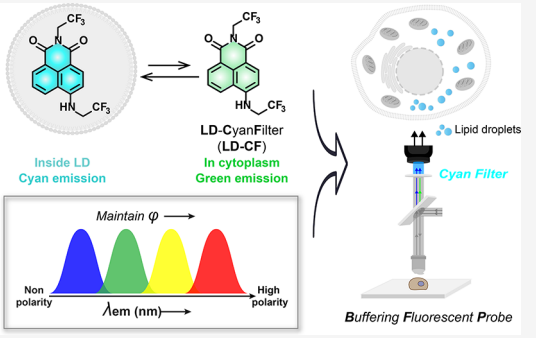


Lipid droplets, ubiquitous organelles spanning from bacteria to mammals, are characterized by a phospholipid monolayer envelope, a neutral lipid core, and specific proteins associated with lipid droplets.[1−4] Serving as a multifunctional organelle, lipid droplets play a crucial role in preserving lipid homeostasis. Additionally, they contribute to membrane synthesis, energy storage, and various cellular processes associated with protein homeostasis.[5,6] Disruptions in the lipid droplet function often contribute to a range of diseases characterized by lipid imbalance,[7] including nonalcoholic fatty liver disease, type 2 diabetes, Alzheimer's disease, cardiovascular disease, and cancer.[8−11] The unique cell biological properties of lipid droplets and their important physiological roles drive research on the correlation between lipid droplet morphology and mechanisms.[12−14] Unfortunately, the highly dynamic processes involved in lipid droplet generation, growth, fusion, and lipid transport still lack comprehensive characterization.[15,16]

Utilizing fluorescent probes for visualizing lipid droplets has emerged as an ideal approach to comprehend the dynamics of lipid droplets and their associated physiological events in living cells.[17−20] In particular, the development of super-resolution imaging techniques allows us to study and decipher physiological processes and molecular mechanisms at the nanoscale.[21] However, most commercially available lipophilic fluorescent probes for lipid droplets, such as Nile Red[22] and BODIPY 493,[23] do not meet the photostability requirements for super-resolution imaging; especially when continuously monitoring the dynamics of very small nascent lipid droplets, probes are often prone to photobleaching. The "buffering strategy" stands out as a highly effective approach to counteract the photobleaching phenomenon commonly observed in probes during super-resolution imaging. This strategy relies on the fact that photobleached fluorophores are efficiently replaced by new intact fluorophores around the target during the imaging process to achieve long-term stable imaging.[24−26] This strategy also imposes a crucial condition—the probe must exhibit a fluorogenic response to the target, meaning that the probe outside the target must remain in a silent fluorescent signal state. We implemented the buffering strategy for the first time in the design of lipid droplet probe **LD-FG**, successfully achieving long-term dynamic super-resolution fluorescence imaging of lipid droplets.[27] **LD-FG** possesses a fitting Clog *P* value, facilitating its aggregation in lipid droplets. Importantly, the hydrogen bond-sensitive

**Received:** January 16, 2024
**Revised:** February 27, 2024
**Accepted:** March 1, 2024
**Published:** March 8, 2024







https://doi.org/10.1021/acs.analchem.4c00292
*Anal. Chem.* 2024, 96, 4709−4715

fluorescence quenching response ensures that the probe outside the lipid droplets remains in a nonfluorescent state, enabling wash-free imaging of the LD.

In this paper, we expanded the application of the buffering strategy to solvatochromic fluorophores (Scheme 1). We

**Scheme 1. (a) LD-CF with a Good Buffering Capacity Enables Cyan Super-Resolution Imaging of LD Using Suitable Emission Filters. (b) Mechanism of LD-CF for LD Dynamic Imaging**

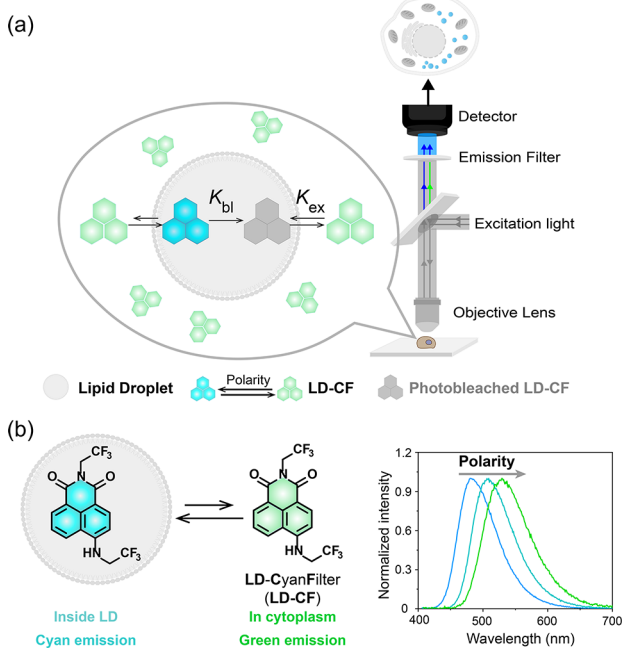


demonstrated that the probe, without the necessity of lipid droplet-targeting fluorogenicity, can also achieve wash-free and prolonged dynamic super-resolution fluorescence imaging of lipid droplets. The fluorescence wavelength of the trifluoroethylamine-substituted naphthylimide derivative **LD-CF** elongates with the rise in microenvironment polarity, while the fluorescence intensity remains constant (Scheme 1 and Figure 1). **LD-CF** exhibits cyan fluorescence in lipid droplets and green fluorescence in the cytoplasm. Leveraging this characteristic, background fluorescence can be eliminated by selecting an appropriate imaging filter (modifying the collection channel range; Scheme 1a). The probe's buffering capacity enhances accuracy and stability for extended imaging periods. It is also worth emphasizing that the fluorescence intensity of the probe remains constant regardless of polarity. This enables the tracing of the lipid transport process during lipid droplet fusion through spatiotemporal imaging of fluorescence intensity, without being influenced by fluctuations in lipid droplet polarity. Using structured illumination microscopy, we examined the targeted transport of lipids during the fusion of lipid droplets. Remarkably, we identified a novel mode of lipid transport between lipid droplets. Contrary to previous studies suggesting directional lipid flow from smaller to larger droplets, leading to fusion into a larger droplet, our observations revealed a different scenario. When two lipid droplets of varying sizes were in close proximity, lipids from the larger droplet partially flowed into the smaller one. Surprisingly, only lipid transport occurred between them, and fusion was not achieved. We believe that further

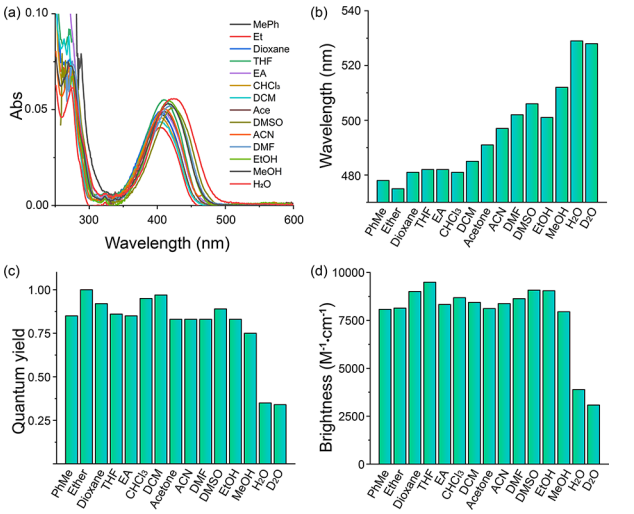


**Figure 1.** (a) UV−vis absorption spectra of 5 $\mu$M **LD-CF** in various solutions. (b) Wavelength of **LD-CF** in various solvents. (c) Quantum yields of **LD-CF** in various solvents. (d) Brightness of **LD-CF** in various solvents.

investigations into lipid droplet dynamics, particularly the transport of lipids between droplets, will yield valuable insights into various metabolic diseases and pathologies intricately linked to lipid droplet biology.[5]

## EXPERIMENTAL SECTION

**General Information.** All $^1$H NMR and $^{13}$C NMR spectra were recorded on a Bruker 400 spectrometer with TMS as the internal standard. Chemical shifts were given in ppm and coupling constants ($J$) in Hz. High-resolution mass spectrometry data were obtained with an HP1100LC/MSD mass spectrometer and LC/Q-TOF MS spectrometer. UV−vis absorption spectra were collected on an Agilent Cary 60 UV−vis spectrophotometer. Fluorescence measurements were performed on an Agilent CARY Eclipse fluorescence spectrophotometer. Confocal images were performed on Olympus FV1000MPE with a microscope IX 71, a 100×/NA 1.40 oil objective lens, LU-NV series laser unit (laser combination: 405, 543, 488, and 635 nm). Super-resolution images were performed by a Nikon N-STORM/SIM 5.0 super-resolution microscope system with a motorized inverted microscope ECLIPSE Ti2-E, a 100×/NA 1.49 oil immersion TIRF objective lens (CFI HP), LU-NV series laser unit (405, 488, 561, and 647 nm), and an ORCA-Flash 4.0 SCMOS camera (Hamamatsu Photonics K.K.).

**Spectroscopic Studies.** **LD-CF** was first prepared as a 2 mM stock solution in DMSO. Samples for spectroscopic analysis were prepared through diluting the stock solution in respective solvents. The concentration of samples was usually prepared at 5 $\mu$M, unless stated otherwise. For fluorescence quantum yield measurements, Coumarin 153 was used as a reference ($\varphi$ = 0.53 in ethanol).

**Cell Culture and Transfection.** HeLa and MCF-7 cells were purchased from the Cell Bank of Type Culture Collection of Chinese Academy of Sciences. Cells were maintained in Dulbecco's modified Eagle's medium (DMEM, Gibco) supplemented with 10% fetal bovine serum (FBS, Hyclone), which were cultured in a humidified atmosphere of 5% $CO_2$/95% air at 37 °C. Before the imaging experiments, cells were seeded on a glass bottom cell culture dish (Nest, polystyrene,


https://doi.org/10.1021/acs.analchem.4c00292
Anal. Chem. 2024, 96, 4709−4715

Φ 15 mm) for 1−2 days to reach 50−80% confluency. The cells were then used for further experiments.

**Confocal Imaging.** The live HeLa or MCF-7 cells were incubated with 0.25−1 μM probes for 0.5−1 h at 37 °C in a 5% $CO_2$ atmosphere. The cells were then directly imaged by using confocal microscopy without washing steps. Ex: 405 nm; collected: 415−465, 425−475, 425−500, 425−525, and 450−550 nm for **LD-CF**. In colocalization experiments, lipid droplets were labeled by LD 540.

**Fluorescence Recovery after Photobleaching Imaging.** Fluorescence recovery after photobleaching (FRAP) experiments was carried out on an Olympus FV1000 MPE confocal laser scanning microscope. Five images were taken before the bleach pulse, and 60 images were taken after the bleaching of regions of interest (ROIs). For the photobleaching process, the ROIs were bleached by laser for 20−30 s. The fluorescence intensity was acquired by the software in the imaging system.

**Preparation of Artificial Lipid Droplets.** We prepared HFE 7500 emulsions in phosphate-buffered saline (PBS) using a vortex mixer, and SDS was used as the surfactant for stabilization. Briefly, 100 μL of HFE 7500 was added to 900 μL of PBS solution containing SDS (20 μM) in a 1.5 mL centrifuge tube, and the mixture was homogenized by using a vortex mixer.

**SIM Imaging.** The live HeLa or MCF-7 cells were incubated with 0.25−1 μM **LD-CF** for 0.5−1 h at 37 °C in a 5% $CO_2$ atmosphere and then were directly imaged using super-resolution microscopy without washing steps.

## RESULTS AND DISCUSSION

**Spectral Characteristics of LD-CF.** We synthesized **LD-CF** through a one-step reaction (Figure S1) and subsequently analyzed its UV−vis absorption and fluorescence spectra in different solvents (Figure 1a and Figure S2). The emission wavelength of **LD-CF** increased from 478 to 528 nm as the solvent polarity rose from toluene to water, accompanied by an increase in the Stokes shift (Figure 1b). **LD-CF** exhibited a moderate quantum yield in water and high fluorescence quantum yields in other solvents, both protic and aprotic (Figure 1c). Even in deuterated water, the quantum yield was nearly consistent with that in water. This suggested that the moderate quantum yield in water was not solely due to hydrogen bonding but likely linked to its solubility in water.[28] Calculations revealed that **LD-CF**'s brightness remained constant with changing solvent polarity, except in water (Figure 1d).

Examining the effects of concentration and system viscosity on **LD-CF**'s fluorescent properties, we observed a linear relationship between fluorescence intensity and concentration in acetonitrile, chloroform, and DMSO. However, a decreasing trend in the fluorescence quantum yield was noted at high concentrations (Figure S3). In the methanol−glycerol system, **LD-CF**'s fluorescence intensity slightly decreased with increased viscosity, while absorbance remained unchanged (Figure S4). In a high-viscosity system (propanetriol), **LD-CF**'s fluorescence intensity exhibited a linear relationship with the concentration, with a slope over 3 times that in the low-viscosity system (Figure S5).

In comparison to the traditional amino-substituted naphthalimide fluorescent dyes, **LD-CF** exhibited a significant increase in the quantum yield across all solvents (Figure S6). Fluorescence quantum yields of **LD-CF** in organic solvents are between 0.8 and 0.9 (Table S1). Notably, unlike traditional amino-substituted naphthalimide, which maintained high quantum yields in nonpolar and polar aprotic solvents but exhibited a significant decrease in polar protic solvents, **LD-CF** consistently maintained relatively stable quantum yields across nonpolar and polar solvents. These results indicate that the inclusion of trifluoroethylamine in naphthalimide has a dual effect: not only does it elevate brightness, but it also ensures a consistent maintenance of fluorescence intensity across various solvents. The enhancement and stabilization of fluorescence intensity by trifluoroethylamine are attributed to the robust electron-attracting ability of trifluoromethyl. This attribute stabilizes the electrons within the fluorophore. Encouragingly, the outcomes of fluorescence lifetime tests align with our initial expectations (Table S2). Considering the complex microenvironments within subcellular organelles, fluorescent probes must possess a high anti-interference capability. To investigate the anti-interference capability of probe **LD-CF**, we added various common interferents to the test solutions and examined changes in the fluorescence spectrum (Figure S7). Experimental results showed that **LD-CF** exhibited minimal fluorescence intensity changes under different interfering substances, demonstrating that it possesses good resistance to interference.

**Fluorescence Imaging with LD-CF.** We then evaluated the performance of **LD-CF** in living cells. Initially, HeLa cells were incubated with **LD-CF** for 30 min and imaged under 405 nm laser excitation. Following the in vitro fluorescence spectra of **LD-CF**, we initially selected a collection channel of 450−550 nm for imaging. The results, as depicted in Figure 2 and

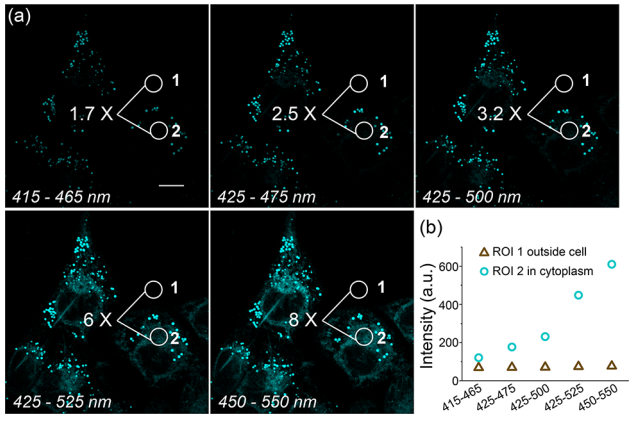


**Figure 2.** (a) Confocal imaging of LDs using **LD-CF** at different collection channels, including 415−465, 425−475, 425−500, 425−525, and 450−550 nm. (b) Mean fluorescence intensity at different collection channels in regions 1 and 2 in panel (a). Scale bar: 10 μm.

Figure S8, revealed that **LD-CF** was distributed in bright dots within the cells, accompanied by background fluorescence in the cytoplasm. Unfortunately, the signal-to-noise ratio of the background fluorescence reached approximately 8.

Considering the significant red-shift in the emission wavelength of **LD-CF** in large polar solvents, we attempted to eliminate background fluorescence in the cytoplasm by altering the collection channel. As anticipated, selecting an appropriate emission filter led to a continuous blue-shift in the collection channel, resulting in a reduction of background fluorescence in the cytoplasm. Fluorescence intensity analysis of the cytoplasm and extracellular regions supported this


https://doi.org/10.1021/acs.analchem.4c00292
Anal. Chem. 2024, 96, 4709−4715

observation. Through collection channel adjustment, the signal-to-noise ratio of background fluorescence in the cytoplasm decreased from 8 to 1.7. It became evident that **LD-CF** was solely distributed in bright dots within HeLa cells. Based on the blue-shifted emission wavelength characteristics of **LD-CF** in a low-polarity environment, we speculate that these bright dot-like areas in the cells corresponded to lipid droplets.

**Colocalization Fluorescence Imaging.** To validate the precise distribution of **LD-CF** in living cells, we conducted colocalization experiments using commercial lipid droplet staining probe LD 540. Merged images demonstrated a significant overlap between the staining of **LD-CF** and commercial dye (Figure 3a). The Pearson colocalization coefficient for **LD-CF** and LD 540 reached 0.8, indicating **LD-CF**'s specific targeting of lipid droplets. To further confirm **LD-CF**'s ability to label intracellular lipid droplets, we incubated HeLa cells with oleic acid, a known inducer of lipid droplet production. Even with increased lipid droplets in cells, **LD-CF** effectively labeled lipid droplets (Figure 3b), as confirmed by colocalization experiments with LD 540. We also explored the possibility of selecting an appropriate collection channel to reduce the cytoplasmic background fluorescence in oleic acid-treated cells. Fortunately, despite the increased background fluorescence, an appropriate emission filter could still minimize interference and meet the requirements of no-wash imaging for lipid droplets. Overall, **LD-CF** proves to be a reliable no-wash imaging tool for further research on lipid droplet physiology, irrespective of the number of lipid droplets present.

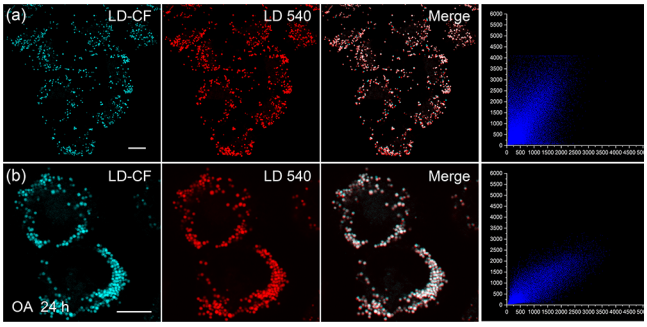


**Figure 3.** (a) Colocalization experiments of lipid droplets in living HeLa cells using **LD-CF** and LD 540. (b) Colocalization experiments of lipid droplets in living HeLa cells treated with 150 $\mu$M OA for 24 h using **LD-CF** and LD 540. Scale bars = 10 $\mu$m.

**Buffer Strategy Enables Photostable Imaging.** Our previous research demonstrated that the appropriate lipophilicity of the probe guaranteed its selective entry into the lipid droplet lumen while allowing the presence of numerous probes in the cytoplasm to form a buffer pool that could be employed to replace photobleached molecules for stable long-term imaging.[27] The mechanism of the buffering fluorescent probe (BFP) strategy has also been elucidated in our previous work; that is, when photobleaching occurred, the excited fluorophore might become oxidized, which increased its hydrophilicity and allowed the photobleached fluorophore to be released from the lipid droplet and enabled an exchange with intact probes in the buffer pool outside of the lipid droplets. **LD-CF** meets all of the requirements for the buffer strategy, with a suitable Clog *P* value and abundant concentration in the cytoplasm, making it ideal for forming a buffer pool. The Clog *P* value of **LD-CF** is 3.661, which is lower than other conventional lipid droplet probes, indicating moderate lipophilicity. Conventional lipid droplet probes may not be retained in the cytoplasm to provide an effective "buffer" due to their high affinity for lipid droplets. Although the **LD-CF** existing in the cytoplasm can still emit fluorescence, in this paper, we adopt the strategy named "cyan filter" based on the different polarities of lipid droplets and cytoplasm and chose to blue-shift the collection channel, which not only satisfied the requirements of reducing the background fluorescence in the cytoplasm but also retained the function of the cytoplasm as a buffer pool. Fluorescence recovery after photobleaching (FRAP) experiments of lipid droplets was performed in HeLa cells to confirm the buffering capacity of **LD-CF**. The experimental results are shown in Figure 4a,b. After irradiating the white circle with a 405 nm laser for 25 s (Figure 4a), the fluorescence of lipid droplets in the circle was quenched, and the fluorescence intensity decreased by 63%. Upon cessation of irradiation, the fluorescence of lipid droplets within the irradiated area recovered rapidly. Analysis of the change in fluorescence intensity of the red circles in Figure 4a shows that the fluorecence intensity of the bleached lipid droplets could be restored to the level before laser irradiation within 1 min. To further demonstrate the "buffering" capacity of **LD-CF**, we repeated the FRAP process with higher staining concentrations (Figure 4c,d). As expected, the fluorescence intensity in the photobleached area decreased by 64%. However, after the laser was turned off, the photobleached lipid droplets returned to the prelaser level within 20 s, in contrast to the recovery time of 1 min at low concentrations. The experimental results showed that fluorescence recovery after photobleaching was significantly accelerated by increasing the staining concentration of intracellular **LD-CF**. This is due to an increase in the number of probes outside the lipid droplets, thus increasing the buffering capacity of the probe pool. The results of the above experiments once again confirmed our previously proposed working mechanism of the buffer strategy. Similarly, we repeated the above experiments in HeLa cells with increased lipid droplets treated with oleic acid (Figure S9).

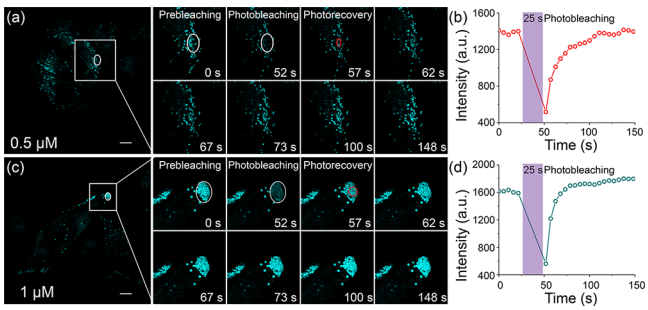


**Figure 4.** (a) Confocal images of 0.5 $\mu$M **LD-CF** in living HeLa cells during photobleaching and photorecovery processes. White circles highlighted the bleaching area. (b) Relative intensity of the red circle in the bleaching area during photobleaching and photorecovery processes in panel (a). (c) Confocal images of 1 $\mu$M **LD-CF** in living HeLa cells during photobleaching and photorecovery processes. White circles highlighted the bleaching area. (d) Relative intensity of the red circle in the bleaching area during photobleaching and photorecovery processes in panel (c). Scale bars = 10 $\mu$m.


https://doi.org/10.1021/acs.analchem.4c00292
Anal. Chem. 2024, 96, 4709−4715

To our delight, the buffering capacity of **LD-CF** was not affected in the presence of a large increase in the number of intracellular lipid droplets. These facts emphasized the good "buffering" capacity and fluorescent properties of **LD-CF** in any cellular state (more or less lipid droplets), which were crucial for high-quality long-term imaging of lipid droplet dynamics.

**Fluorescence Imaging of Artificial Lipid Droplets with LD-CF.** Chemical systems capable of replicating cell behavior can help elucidate the complexity of biological systems. In recent years, there has been a growing interest among researchers in the use of artificial lipid droplet systems to study the mechanisms of lipid droplet formation and kinetics.[29−32] To better understand the dynamic process of lipid droplets, we first mimicked cellular lipid droplets to construct artificial lipid droplets for imaging. We prepared HFE 7500 emulsions in phosphate-buffered saline (PBS) by using a vortex mixer, and SDS was used as a surfactant for stabilization (Figure 5). The size of the resulting droplets was

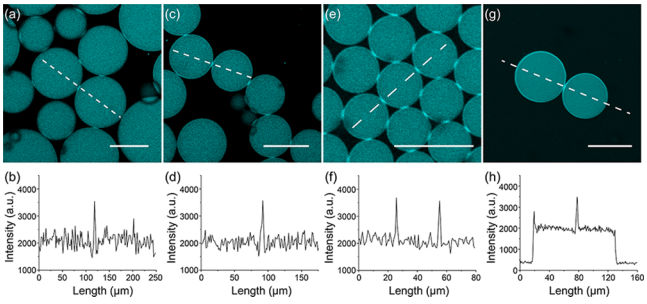


**Figure 5.** Confocal images of the synthetic lipid droplets stained with different concentrations of **LD-CF**, 10 $\mu$M **LD-CF** in panels (a, c, e) and 20 $\mu$M **LD-CF** in panel (g). (b, d, f, h) Relative intensity at synthetic lipid droplet contact sites (white dotted line) in panels (a, c, e, g). Scale bars = 100 $\mu$m.

controlled in the range of 30−150 $\mu$m by adjusting the mixing time. We stained droplets with 10 $\mu$M **LD-CF** and imaged them using confocal microscopy. As shown in Figure 5a−f, **LD-CF** effectively labeled the artificial lipid droplets and distributed uniformly within the droplets. Surprisingly, we observed that fluorescence intensity was markedly increased at the contact sites when two droplets came into close proximity. We hypothesized that when two droplets were pressed against each other, the monolayers surrounding the droplets were squeezed to form a more densely packed monolayer, leading to an increased local concentration of **LD-CF** and thus significantly enhanced fluorescence at the contact site. Moreover, the fluorescence increase at the contact site was more pronounced with smaller-sized droplets, likely due to the greater surface tension of smaller droplets resulting in a more compact monolayer. In addition, we observed similar phenomena when the staining concentration of **LD-CF** was increased to 20 $\mu$M (Figure 5g,h). Therefore, we concluded that the local fluorescence intensity at the contact site of **LD-CF** labeled droplets increased with a higher **LD-CF** concentration upon droplet−droplet contact. The results obtained with model lipid droplets give us confidence to move forward with studying droplet dynamics by labeling cellular lipid droplets.

**Visualizing the Lipid Transport Dynamic Process between LD Pairs in Live Cells.** Adequate energy storage is crucial for maintaining a healthy life. An important function of lipid droplets is to store energy in the form of neutral lipids and to release fatty acids in the event of an energy deficiency. The energy storage capacity, reflected by lipid droplet size,[33] is controlled by two molecular pathways: neutral lipid synthesis and lipid droplet fusion. The actual effect of lipid droplet fusion can be considered as lipid transport between lipid droplet pairs. Therefore, visualizing the lipid transport process between lipid droplet pairs can contribute to a better understanding of lipid droplet dynamics. Given the ability of **LD-CF** to dynamically label lipid droplets and its performance as a buffer probe for long-term imaging, we aim to observe lipid transport during lipid droplet fusion through super-resolution live-cell imaging. Previous studies[34−38] have shown two primary mechanisms of lipid droplet fusion: LD coalescence and atypical fusion mediated by CIDE proteins were also considered ripening. LD coalescence involves the formation of continuity between the phospholipid monolayers of two droplets, leading to the subsequent merging of the internal lipid droplets. It has been widely assumed that LD coalescence is rarely observed under physiological conditions. The rationale is that it occurs spontaneously due to altered phospholipid composition in the droplet monolayer, either insufficient levels of LD-stabilizing phosphatidylcholine or accumulation of fusogenic phosphatidic acid.[39,40] However, our previous systematic experimental results suggest that LD coalescence may not be a "rare" event and can occur frequently in living cells (Figure S11). Here, we stained HeLa cells with **LD-CF** and observed LD coalescence under SIM. As shown in Figure 6a, two adjacent droplets started to be pressed against each other at 20 s and formed a dumbbell shape. At 52 s, a bright oval region emerged and expanded in the center of the dumbbell-shaped droplet. The oval region continued enlarging and moving to one side. Analysis of fluorescence intensity profiles along the diameter of dumbbell-shaped droplets was consistent with observations (Figure 6b), showing an increasing intensity in the middle region over time. The fluorescence intensity in the middle region reached similar levels as the two sides at 44 s. As coalescence proceeded, the intensity kept increasing and the position of maximal intensity shifted to one side. Unfortunately, due to the long duration of the process, we were not able to capture the entire process to observe the formation of a spherical fused lipid droplet. Nonetheless, our results suggested that neutral lipids appeared to flow from one droplet to the other during coalescence. In contrast, lipid transport during the ripening process showed distinct behaviors. When two droplets came into close proximity, CIDE proteins on the droplet surface accumulated at the contact site, and lipids always transferred unidirectionally from the smaller donor droplet to the larger acceptor droplet. Since the interior pressure in the smaller droplet is higher than in the larger LD, this pressure difference is widely considered in the literature to be the driving force for lipid transfer during fusion, suggesting that lipid transfer kinetics may have important fluid dynamic components. Moreover, it has been reported that the "acceptor" LD receiving lipids from other droplets in early fusion events can later become a "donor" to transfer lipids to another acceptor in subsequent fusions. Fortunately, with the "buffering probe" **LD-CF** and SIM, we were able to fully visualize this entire dynamic process. As the imaging time increased, two adjacent droplets underwent fusion, with lipid transfer occurring from the smaller to the larger one. The fused droplet continued to


https://doi.org/10.1021/acs.analchem.4c00292
Anal. Chem. 2024, 96, 4709−4715

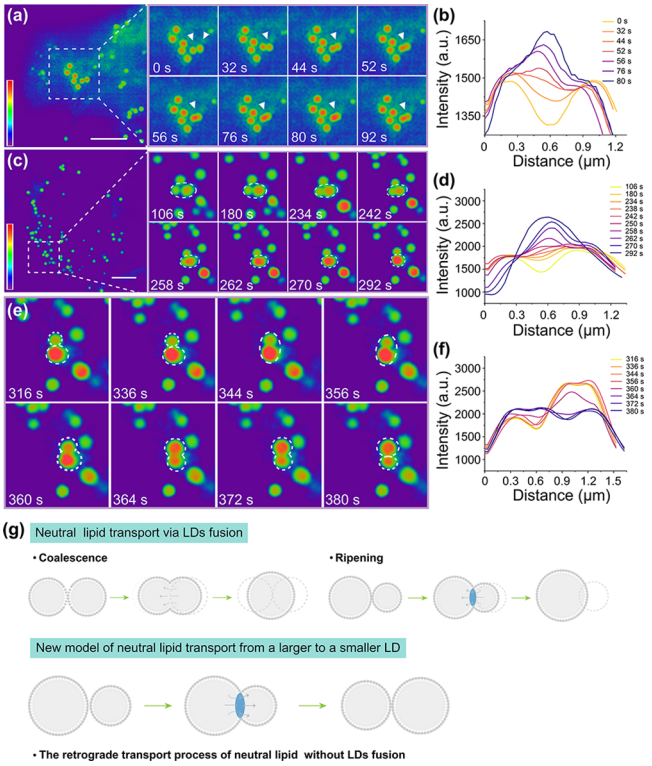


**Figure 6.** (a) SIM image of living HeLa cells with 0.5 $\mu$M **LD-CF** and the locally enlarged images of the boxed region for dynamic LD coalescence processes. (b) Relative intensity of the red line during LD coalescence processes in panel (a). (c) SIM image of living HeLa cells with 0.5 $\mu$M **LD-CF** and the locally enlarged images of the boxed region for dynamic LD fusion processes. (d) Relative intensity of the red line during LD coalescence processes in panel (c). (e) Locally enlarged SIM image of the boxed region in panel (c) for the transport process of neutral lipids. (f) Relative intensity of the red line during LD coalescence processes in panel (e). (g) Model of the dynamic transport process of neutral lipids between LD pairs.

participate in further fusion events, increasing in volume until no further fusion was observed at a certain size. Interestingly, we observed a novel lipid transport process between the LD pairs during fusion, as shown in Figure 6c–f; two adjacent droplets first fused into a larger droplet. Subsequently, instead of the expected unidirectional lipid transfer from the smaller to the larger droplet, parts of lipids in the larger droplet moved to the smaller droplet after their contact, which caused the larger droplet to shrink and the smaller one to grow in volume without them undergoing fusion during imaging, solely through lipid transport. All these results demonstrate the ability of **LD-CF** as a fluorescent probe to visualize lipid transport dynamics between LD pairs in live cells (Figure 6g). Although many mysteries still exist regarding droplet dynamics, especially the biological implications of material transport during fusion, the excellent buffering capability of **LD-CF** encourages us to utilize it for long-term live-cell imaging of droplet dynamics in future work.

## CONCLUSIONS

We have further substantiated that the development of buffering, photostable fluorescent probes present a promising general strategy for analyzing organelle dynamics through super-resolution microscopy. The buffering probe **LD-CF**, which we introduced, facilitates wash-free, long-term super-resolution imaging of lipid droplets. This capability stems from its moderate lipophilicity and polarity-sensitive property, harnessed through the "cyan filter" strategy. Using **LD-CF**, we successfully monitored lipid transport during lipid droplet fusion over an extended period, uncovering a novel mode of lipid flow from larger to smaller droplets. We posit that the amalgamation of buffering strategies with super-resolution imaging techniques will provide robust support for deciphering and understanding the dynamic physiological processes of organelles in the future.

## ASSOCIATED CONTENT

### Supporting Information

The Supporting Information is available free of charge at https://pubs.acs.org/doi/10.1021/acs.analchem.4c00292.

General experimental information, methods, Figures S1–S14, Tables S1 and S2, and $^{1}$H, $^{13}$C, and HRMS spectra for **LD-CF** (PDF)

## AUTHOR INFORMATION


### Corresponding Authors

**Qinglong Qiao** − *Dalian Institute of Chemical Physics, Chinese Academy of Sciences, Dalian 116023, China*; Email: qqlqiao@dicp.ac.cn

**Zhaochao Xu** − *Dalian Institute of Chemical Physics, Chinese Academy of Sciences, Dalian 116023, China; School of Chemistry, Dalian University of Technology, Dalian 116024, China*; orcid.org/0000-0002-2491-8938; Email: zcxu@dicp.ac.cn

### Authors

**Ning Xu** − *Dalian Institute of Chemical Physics, Chinese Academy of Sciences, Dalian 116023, China; School of Chemistry, Dalian University of Technology, Dalian 116024, China*

**Xiangning Fang** − *Dalian Institute of Chemical Physics, Chinese Academy of Sciences, Dalian 116023, China*

**Guangying Wang** − *Dalian Institute of Chemical Physics, Chinese Academy of Sciences, Dalian 116023, China*

**Kai An** − *Dalian Institute of Chemical Physics, Chinese Academy of Sciences, Dalian 116023, China*

**Wenchao Jiang** − *Dalian Institute of Chemical Physics, Chinese Academy of Sciences, Dalian 116023, China*

**Jin Li** − *Dalian Institute of Chemical Physics, Chinese Academy of Sciences, Dalian 116023, China*

Complete contact information is available at: https://pubs.acs.org/10.1021/acs.analchem.4c00292


### Author Contributions

N.X., X.F., G.W., K.A., W.J., and J.L. conducted the experiments, Q.Q. and Z.X. designed the experiments, and N.X. and Z.X. wrote the manuscript. All authors have given approval to the final version of the manuscript.

### Notes

The authors declare no competing financial interest.

## ACKNOWLEDGMENTS

This work is supported by the National Natural Science Foundation of China (22278394, 22078314, and 21908216) and Dalian Institute of Chemical Physics (DICPI202227 and DICPI202142).

## REFERENCES


(1) Krahmer, N.; Guo, Y.; Farese, R. V., Jr; Walther, T. C. *Cell* **2009**, *139*, 1024−1024.
(2) Boschi, F.; Rizzatti, V.; Zamboni, M.; Sbarbati, A. *Exp. Cell Res.* **2015**, *336*, 253−262.
(3) Yang, H.; Galea, A.; Sytnyk, V.; Crossley, M. *Curr. Opin. Cell Biol.* **2012**, *24*, 509−516.
(4) Guo, Y.; Walther, T. C.; Rao, M.; Stuurman, N.; Goshima, G.; Terayama, K.; Wong, J. S.; Vale, R. D.; Walter, P.; Farese, R. V. *Nature* **2008**, *453*, 657−661.
(5) Thiam, A. R.; Farese, R. V., Jr; Walther, T. C. *Nat. Rev. Mol. Cell Biol.* **2013**, *14*, 775−786.
(6) Walther, T. C.; Farese, R. V., Jr *Annu. Rev. Biochem.* **2012**, *81*, 687−714.
(7) Dalhaimer, P. *Cells* **2019**, *8*, 974.
(8) Liu, C.-C.; Kanekiyo, T.; Xu, H.; Bu, G. *Nat. Rev. Neurol.* **2013**, *9*, 106−118.
(9) Cruz, A. L. S.; Barreto, E. D. A.; Fazolini, N. P. B.; Viola, J. P. B.; Bozza, P. T. *Cell Death Dis.* **2020**, *11*, 105.
(10) Younossi, Z.; Tacke, F.; Arrese, M.; Sharma, B. C.; Mostafa, I.; Bugianesi, E.; Wong, V. W.-S.; Yilmaz, Y.; George, J.; Fan, J.; Vos, M. B. *Hepatology* **2019**, *69*, 2672−2682.
(11) Gluchowski, N. L.; Becuwe, M.; Walther, T. C.; Farese, R. V., Jr *Nat. Rev. Gastroenterol. Hepatol.* **2017**, *14*, 343−355.
(12) Olzmann, J. A.; Carvalho, P. *Nat. Rev. Mol. Cell Biol.* **2019**, *20*, 137−155.
(13) Son, S.-H.; Park, G.; Lim, J.; Son, C. Y.; Oh, S. S.; Lee, J. Y. *Nat. Commun.* **2022**, *13*, 3612.
(14) Meyers, A.; Weiskittel, T. M.; Dalhaimer, P. *Lipids* **2017**, *52*, 465−475.
(15) Olofsson, S.-O.; Boström, P.; Andersson, L.; Rutberg, M.; Perman, J.; Borén, J. *Biochim. Biophys. Acta* **2009**, *1791*, 448−458.
(16) Barneda, D.; Christian, M. *Curr. Opin. Cell Biol.* **2017**, *47*, 9−15.
(17) Wang, J.; Han, X. *TrAC, Trends Anal. Chem.* **2019**, *121*, No. 115697.
(18) Jüngst, C.; Klein, M.; Zumbusch, A. *J. Lipid Res.* **2013**, *54*, 3419−3429.
(19) Lee, H. W.; Lee, I.-J.; Lee, S.-J.; Kim, Y. R.; Kim, H. M. *ACS Sens.* **2022**, *7*, 1027−1035.
(20) Danylchuk, D. I.; Jouard, P.-H.; Klymchenko, A. S. *J. Am. Chem. Soc.* **2021**, *143*, 912−924.
(21) Taki, M.; Kajiwara, K.; Yamaguchi, E.; Sato, Y.; Yamaguchi, S. *ACS Mater. Lett.* **2021**, *3*, 42−49.
(22) Greenspan, P.; Mayer, E. P.; Fowler, S. D. *J. cell biol.* **1985**, *100*, 965−973.
(23) Qiu, B.; Simon, M. *Bio-Protoc.* **2016**, *6*, No. e1912.
(24) Jiang, W.; Chen, J.; An, K.; Bao, P.; Qiao, Q.; Liu, X.; Xu, Z. *Green. Chem. Eng.* **2023**, *4*, 387−392.
(25) Chen, J.; Liu, W.; Fang, X.; Qiao, Q.; Xu, Z. *Chin. Chem. Lett.* **2022**, *33*, 5042−5046.
(26) Chi, W.; Chen, J.; Liu, W.; Wang, C.; Qi, Q.; Qiao, Q.; Tan, T. M.; Xiong, K.; Liu, X.; Kang, K.; Chang, Y. T.; Xu, Z.; Liu, X. *J. Am. Chem. Soc.* **2020**, *142*, 6777−6785.
(27) Chen, J.; Wang, C.; Liu, W.; Qiao, Q.; Qi, H.; Zhou, W.; Xu, N.; Li, J.; Piao, H.; Tan, D.; Liu, X.; Xu, Z. *Angew. Chem., Int. Ed.* **2021**, *60*, 25104−25113.
(28) Dobretsov, G.; Syrejschikova, T.; Smolina, N. *Biophysics* **2014**, *59*, 183−188.
(29) Wang, Y.; Zhou, X.-M.; Ma, X.; Du, Y.; Zheng, L.; Liu, P. *ACS Nano* **2016**, *10*, 3312−3322.
(30) Wang, X.; Huang, Y.; Lin, Y.; Chen, H.; Li, J.; Zhao, C.; Liu, X.; Yang, L.; Huang, X. *CCS Chem.* **2021**, *3*, 2782−2794.
(31) Eördögh, Á.; Paganini, C.; Pinotsi, D.; Arosio, P.; Rivera-Fuentes, P. *ACS Chem. Biol.* **2020**, *15*, 2597−2604.
(32) Chen, H.; Li, W.; Lin, Y.; Wang, L.; Liu, X.; Huang, X. *Angew. Chem., Int. Ed.* **2020**, *59*, 16953−16960.
(33) Yu, J.; Li, P. *Sci. China: Life Sci.* **2017**, *60*, 46−56.
(34) Lyu, X.; Wang, J.; Wang, J.; Yin, Y.-S.; Zhu, Y.; Li, L.-L.; Huang, S.; Peng, S.; Xue, B.; Liao, R.; Wang, S.-Q.; Long, M.; Wohland, T.; Chua, B. T.; Sun, Y.; Li, P.; Chen, X.-W.; Xu, L.; Chen, F.-J.; Li, P. *Dev. Cell* **2021**, *56*, 2592−2606.
(35) Wu, L.; Zhou, L.; Chen, C.; Gong, J.; Xu, L.; Ye, J.; Li, D.; Li, P. *Sci. China: Life Sci.* **2014**, *57*, 107−116.
(36) Gao, G.; Chen, F.-J.; Zhou, L.; Su, L.; Xu, D.; Xu, L.; Li, P. *Biochim. Biophys. Acta, Mol. Cell Biol. Lipids* **2017**, *1862*, 1197−1204.
(37) Wilfling, F.; Haas, J. T.; Walther, T. C.; Farese, R. V., Jr *Curr. Opin. Cell Biol.* **2014**, *29*, 39−45.
(38) Mau, K. H. T.; Karimlou, D.; Barneda, D.; Brochard, V.; Royer, C.; Leeke, B.; de Souza, R. A.; Pailles, M.; Percharde, M.; Srinivas, S.; Jouneau, A.; Christian, M.; Azuara, V. *Nat. Commun.* **2022**, *13*, 3861.
(39) Brasaemle, D. L. *Cell Metab.* **2011**, *14*, 437−438.
(40) Fei, W.; Shui, G.; Zhang, Y.; Krahmer, N.; Ferguson, C.; Kapterian, T. S.; Lin, R. C.; Dawes, I. W.; Brown, A. J.; Li, P.; Huang, X.; Parton, R. G.; Wenk, M. R.; Walther, T. C.; Yang, H. *PLoS Genet.* **2011**, *7*, No. e1002201.



https://doi.org/10.1021/acs.analchem.4c00292
*Anal. Chem.* 2024, 96, 4709−4715